

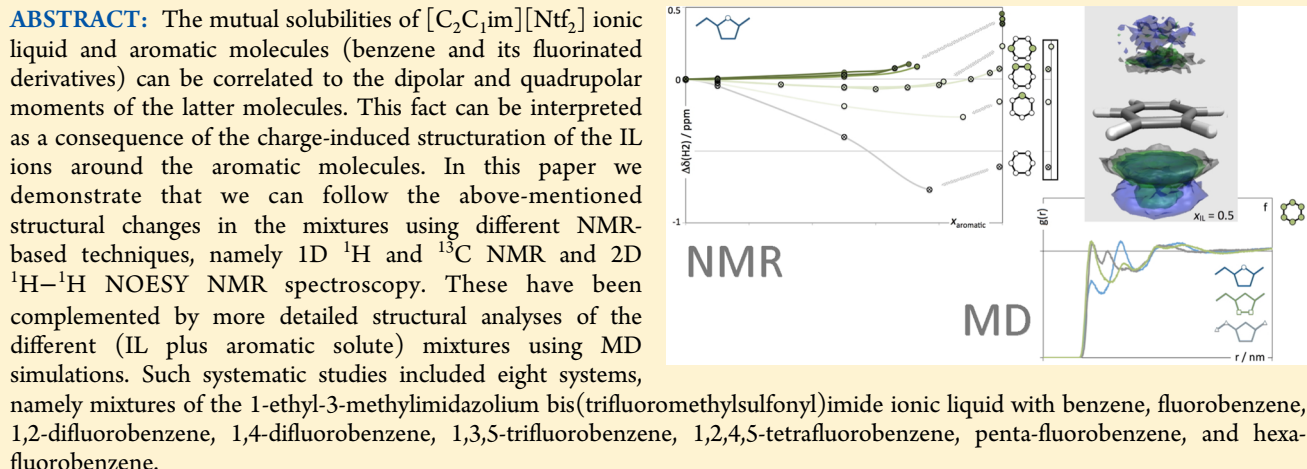
Charge Templates in Aromatic Plus Ionic Liquid Systems Revisited: NMR Experiments and Molecular Dynamics Simulations

Nuno Dias,[‡] Karina Shimizu,[†] Pedro Morgado,[†] Eduardo J. M. Filipe,[†] José N. Canongia Lopes,^{*,†} and Fabián Vaca Chávez^{*,§}

[†]Centro de Química Estrutural (CQE), Instituto Superior Técnico, Universidade de Lisboa, 1049-001 Lisboa, Portugal

[‡]Departamento de Física, Instituto Superior Técnico, Universidade de Lisboa, 1049-001 Lisboa, Portugal

[§]Centro de Física da Matéria Condensada (CFMC), Universidade de Lisboa, 1649-004 Lisboa, Portugal



INTRODUCTION

In recent years we have used ab initio calculations and molecular dynamics (MD) simulations to investigate the mutual solubility of different molecular species (MS) and ionic liquids (ILs).

One of our first studies centered on the unusual phase behavior of mixtures of an IL (1-ethyl-3-methylimidazolium bis(trifluoromethylsulfonyl)imide, $[C_2C_1im][Ntf_2]$) plus benzene and its fluorinated derivatives.¹ By changing the number and position of the fluorine atoms substituting the aromatic ring of benzene, we were able to show, using MD-based spatial distribution functions, that the ions of $[C_2C_1im][Ntf_2]$ acted as charge templates for the dipole and/or quadrupole moments of the aromatic molecules. In other words, the mutual solubility of those molecular species and ILs could be correlated to the ability of the IL ions to surround the solute molecules in a way that matched the electrical field of the latter, or, conversely, a given solute molecule was more soluble in the ionic liquid if it could find a position/orientation within the IL polar network that suitably matched its electronic density distribution.

Such studies were then extended to other classes of ILs and molecular compounds (haloalkanes, water, octanol, ethers),² in order to interpret at a molecular level the fluid phase behavior of the corresponding IL+MS systems. It was found that in most cases the ion–molecule interactions that define the complex behavior of such systems can be correlated to (i) the electronic density makeup of the molecular species (presence or absence

of important dipole and quadrupole moments, coupling between dipole moments); (ii) the conformational flexibility of the molecular ions that compose the ionic liquid and the concomitant mobility of the polar network formed by them; and (iii) the presence of any functional groups in the ions or in the molecules that may introduce extra specific interactions.

On the other hand, several NMR studies have been conducted by different authors^{3–8} to probe the interactions between ionic liquid ions and molecular species dissolved in them, such as water, organic solvents and nucleobases. These studies involved multinuclear 1D and also more sophisticated 2D NMR spectroscopy. One of the advantages of such methods is that information about each interaction center in the ions or the molecular species can be monitored individually as the composition of the (IL+MS) is changed.

In this work we revisit the original IL + aromatic systems in order to corroborate and extend the initial findings suggested by MD simulations. We have now used NMR spectroscopy on most of the systems to obtain information on the interactions between individual atoms on the ions and in the molecular species and how these match the original averaged-out spatial distribution functions and also newly MD-based pair radial distribution functions between selected interaction centers in

Received: March 29, 2014

Revised: May 7, 2014

Published: May 9, 2014

the mixtures' components. By coming full circle, we hope to give a more complete picture of the solvation mechanisms characteristic of these (IL+MS) systems.

■ EXPERIMENTAL SECTION

Materials. The ionic liquid 1-ethyl-3-methylimidazolium bis(trifluoromethylsulfonyl)imide, $[C_2C_1\text{im}][\text{Ntf}_2]$, was purchased from Iolitec (>99% purity) and then dried under vacuum (~100 Pa), vigorous stirring, and moderate temperature (~320 K) for more than 24 h before each use. Benzene was purchased from Panreac, with 99.5% purity. All fluorinated compounds were purchased from Alfa Aesar: fluorobenzene, 1,4-difluorobenzene, 1,2,4,5-tetrafluorobenzene, and hexafluorobenzene with purity levels better than 99%; 1,2-difluorobenzene, 1,3,5-trifluorobenzene, and pentafluorobenzene with purity levels better than 98%. All compounds were dried for several weeks over freshly activated type-3 Å molecular sieves supplied by Aldrich.

Sample Preparation. The $[C_2C_1\text{im}][\text{Ntf}_2]$ + aromatic molecule mixtures were prepared by weight in screw-cap vials, using an analytic balance (Ohaus) with a resolution of 0.01 mg. In the cases where the systems presented liquid–liquid immiscibility in a given composition range, a vial was prepared containing both phases in equilibrium. Appropriate amounts of both components were mixed in the vial in order to obtain similar volumes of the two liquid phases. The vial was agitated and then left undisturbed for several days in order to ensure complete decantation and a correct collection (using a syringe) of two samples corresponding to each one of the saturated phases. The composition of the saturated phases was estimated based on the experimental results by Shiflett and Yokozeki.⁹ It should be mentioned that, although the mole fraction of some benzene derivatives in the aromatic-rich samples is nominally 1.0, the “infinite-dilution” concentration of ionic liquid in these samples was always high enough to allow the detection of the corresponding peaks in the ^1H NMR spectrum, by using an adequate number of scans (cf. next subsection).

NMR Measurements. The NMR measurements were performed on a 7.05 T Bruker AVANCE II spectrometer operating at 300 MHz Larmor frequency for ^1H and 75 MHz for ^{13}C . The ^1H spectra were obtained after a 90° pulse with a pulse $t_{90} = 12 \mu\text{s}$. The number of scans ranged from 16 to 512 depending on the concentrations with a relaxation delay (d_1) of 3 s. The ^{13}C spectra were acquired after $t_{90} = 11 \mu\text{s}$ and $d_1 = 2$ s. The proton decoupled ^{13}C spectra were obtained using the standard WALTZ-16 decoupling sequence. These measurements have been completed by performing 2D ^1H – ^1H NOESY with a mixing time between 600 and 800 ms.

Molecular Dynamics Simulations. The $[C_2C_1\text{im}][\text{Ntf}_2]$ ionic liquid was represented by the CL&P force field,^{10,11} an extension of the OPLS-AA model.¹² Benzene and its derivatives were also modeled within the OPLS framework using the parametrization proposed by Jorgensen¹² and the CHelpG charges obtained in a previous work.¹ All simulations were performed using molecular dynamics algorithms, implemented in the DL_POLY program.¹³

Three types of mixture were considered: the IL-rich mixtures ($x_{\text{IL}} = 0.75$) were composed of 192 $[C_2C_1\text{im}][\text{Ntf}_2]$ ion pairs and 64 solute molecules; the equimolar mixtures contained 128 IL ion pairs and 128 solute molecules; finally, “IL at infinite dilution” mixtures contained 1 ion pair and 420 solute molecules.

In the case of all benzene and hexafluorobenzene mixtures and most 1,2-difluorobenzene mixtures, we started from low-density initial configurations. All mixtures were pre-equilibrated under $N\text{-}p\text{-}T$ ensemble conditions for 500 ps at 300 K using a Nosé–Hoover thermostat and barostat with time constants of 0.5 and 2 ps, respectively. Electrostatic interactions were treated using the Ewald summation method considering six reciprocal-space vectors, and repulsive-dispersive interactions were explicitly cut off at 1.6 nm (long-range corrections were applied assuming the system had a uniform density beyond this cutoff radius). The final configuration of the pre-equilibrated hexafluorobenzene mixture ($x_{\text{IL}} = 0.75$) system was used to generate the initial configuration of the 1,2-difluorobenzene ($x_{\text{IL}} = 0.75$) mixture and further simulation runs of 300 ps were used to produce a new re-equilibrated system.

Several (about 6) consecutive production stages of 1.0 ns each were performed for all pre-equilibrated mixtures. Finally, 3000 configurations were stored from production runs of 600 ps for each one of the possible 9 systems. Successive 300 ps runs of each system showed no drift in the corresponding equilibrium properties at this stage. The stored configurations for each system were used to generate the presented spatial distribution functions (SDFs).

■ DISCUSSION

Our previous work on $[C_2C_1\text{im}][\text{Ntf}_2]$ plus benzene and its fluorinated derivatives¹ has shown that the ions of the ionic liquid will always charge-template the electric dipole/quadrupole moments generated by the aromatic molecules in a very effective manner. In the case of benzene, the cations adopt axial positions relative to the aromatic plane, whereas in hexafluorobenzene the cations will surround the aromatic plane of the MSs at equatorial positions. In terms of ^1H NMR, this has a profound effect in terms of shielding/deshielding of the magnetic moments of the hydrogen nuclei in the imidazolium cation: in the polar positions of an aromatic plane there are always strong upfield shifts (shielding effects causing deviations to smaller δ values), whereas at the equatorial positions of the plane, there are strong downfield shifts (deshielding effects causing deviations to larger δ values). Moreover, when the cations start to interact at the equatorial positions of the aromatic plane, they do so at the fluorine-substituted positions. This interaction with the electronegative fluorine atoms can also lead to additional deshielding shifts in the corresponding NMR signals.

The NMR data compiled in Figure 1 confirms the charge template effect around the different aromatic molecules. The figure shows the differences in the proton chemical shift ($\Delta\delta$) of the H2 hydrogen of the imidazolium cation (cf. Scheme 1) in the mixtures and the corresponding values in the pure ionic liquid, as a function of the aromatic solute mole fraction. As can be seen, when benzene is progressively added to the pure IL, the shifts deviate to lower values (the cations are positioned above and below the aromatic plane and will feel strong shielding shifts); when the added aromatic solutes are more fluorinated, the cations will start to move toward more equatorial positions of the corresponding aromatic planes, and the NMR shifts will become progressively more downfield (positive $\Delta\delta$, deshielded values).

The H2 hydrogen is the most interactive site (the most acidic proton) of the imidazolium cation, which means that any perturbation in the polar network of the ionic liquid will be felt with particular intensity at this position. In other words, the

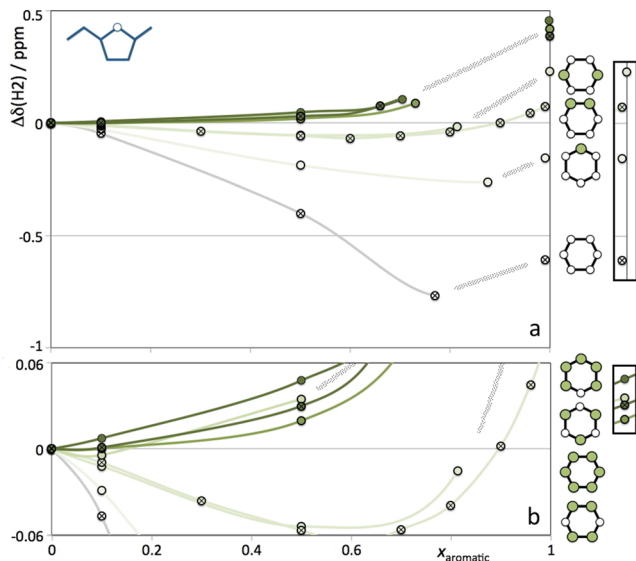
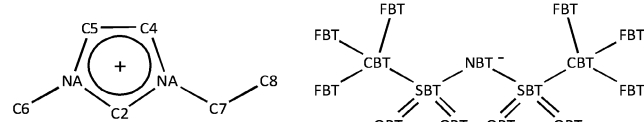


Figure 1. Deviations of the ^1H NMR shifts of the $\text{H}2$ proton of $[\text{C}_2\text{C}_1\text{im}]^+$, $\Delta\delta(\text{H}2)$, as a function of the concentration of eight different aromatic solutes (benzene and seven fluorinated benzenes), x_{aromatic} , in (IL+aromatic) mixtures. The green and white circles in the hexagonal schematics represent the fluorinated and hydrogenated positions of the different solutes. The insets at the right side of the graphs show the correspondence between each schematic and its line/symbol. The bottom panel (b) is a zoom of the top one (a) for deviations with small intensity. The shaded line segments represent the immiscibility windows for each mixture.

Scheme 1. Structural Formulas and Nomenclature of the $[\text{C}_2\text{C}_1\text{im}]^+$ and $[\text{Ntf}_2]^-$ Ions^a



^aThe hydrogen atoms of the cation are mentioned in the text taking into account the number of the carbon atom to which they are attached.

competition between the anions and the aromatic solutes for interactions at that position will be particularly fierce and can explain the different trends observed for the δ shifts along the mixtures' composition range (cf. below). The interruption in the lines in the graph by shaded segments represent the immiscibility windows present in the systems studied, and the points on each side of the immiscibility gap correspond to the saturated phases at equilibrium. Mixtures of $[\text{C}_2\text{C}_1\text{im}][\text{Ntf}_2]$ and 1,2-difluorobenzene exhibit complete miscibility between the two components.

Figure 2a–c shows the same shift differences for the different protons of the cation when the $[\text{C}_2\text{C}_1\text{im}][\text{Ntf}_2]$ IL is progressively diluted with hexafluorobenzene, 1,2-difluorobenzene, and benzene/deuterobenzene, respectively. Overall, the behavior of the different protons in the cation can be sorted into three groups: (i) the $\text{H}2$ proton, (ii) the $\text{H}4$ and $\text{H}5$ protons, and (iii) the $\text{H}6$, $\text{H}7$, and $\text{H}8$ protons. The first two groups are the aromatic hydrogen atoms directly connected to the imidazolium ring; the latter comprises aliphatic hydrogen atoms connected to the methyl and ethyl groups of the cation. Figure 2 shows that the three groups behave quite differently.

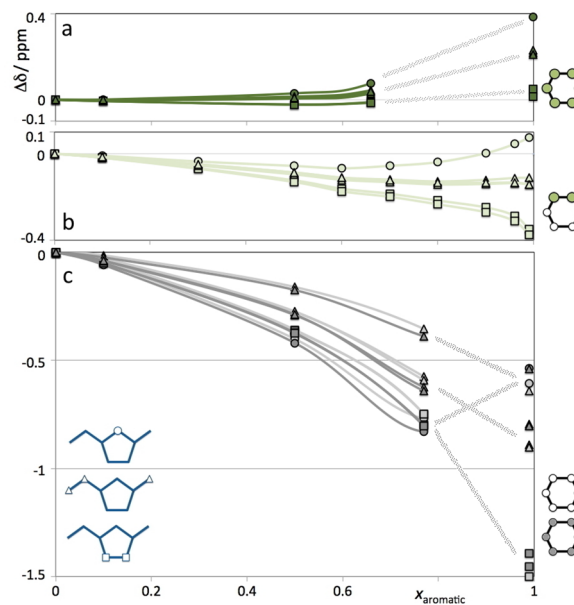


Figure 2. Deviations of the ^1H NMR shifts of the different protons of $[\text{C}_2\text{C}_1\text{im}]^+$, $\Delta\delta$, as a function of the concentration of four different aromatic solutes in (IL+aromatic) mixtures. The blue insets designate the positions of the different protons in the cation: $\text{H}2$ (circles), $\text{H}4/\text{H}5$ (squares), and $\text{H}6/\text{H}7/\text{H}8$ (triangles). The four solutes are benzene and deuterobenzene (bottom graph, c), 1,2-difluorobenzene (middle, b) and hexafluorobenzene (top, a). Benzene and deuterobenzene data are represented in light gray and dark gray, respectively. The shaded line segments represent the immiscibility windows for each mixture. Hexagonal schematics are as in Figure 1.

In the case of the benzene/deuterobenzene mixtures (Figure 2c), the aromatic protons in the mixtures exhibit larger shielding shifts than their aliphatic counterparts. The $([\text{C}_2\text{C}_1\text{im}][\text{Ntf}_2] + \text{C}_6\text{H}_6/\text{C}_6\text{D}_6)$ mixtures show liquid–liquid demixing at room temperature between 0.75 aromatic mole fraction and the (almost) pure aromatic molecule⁹ (shaded areas in the graph). Thus, the points on the right side of the figure correspond to signals from imidazolium cations at almost infinite dilution conditions in the benzene solvent. Whereas no large difference is shown between the aromatic protons on the IL-rich side of the graph, the $\text{H}2$ proton at infinite dilution shows a much smaller shielding shift than its $\text{H}4/\text{H}5$ counterparts.

In the case of the $[\text{C}_2\text{C}_1\text{im}][\text{Ntf}_2] + 1,2$ -difluorobenzene mixtures (that exhibit complete miscibility over the entire concentration range, as attested by the large number of experimental data covering all of it), the $\text{H}2$ protons exhibit small shielding shifts as the aromatic molecule concentration is increased. At higher concentrations, these turn into small deshielding shifts. The aliphatic protons show intermediate shielding shifts and the $\text{H}4/\text{H}5$ protons display the largest shielding shifts. This neat separation between the behavior of the three aromatic protons of the imidazolium ring (already hinted at in the case of the infinite dilution point in the benzene mixtures) is quite unexpected and provides novel insights concerning the relative orientation of the ions and the aromatic molecules that had not been addressed in the aforementioned MD study.¹

Finally, in the case of the $([\text{C}_2\text{C}_1\text{im}][\text{Ntf}_2] + \text{hexafluorobenzene})$ mixtures (Figure 2a), most shifts are deshielding, and the order $\text{H}2 > \text{H}6-\text{H}8 > \text{H}4/\text{H}5$ already observed in Figure 2b is retained. There is also an immiscibility window

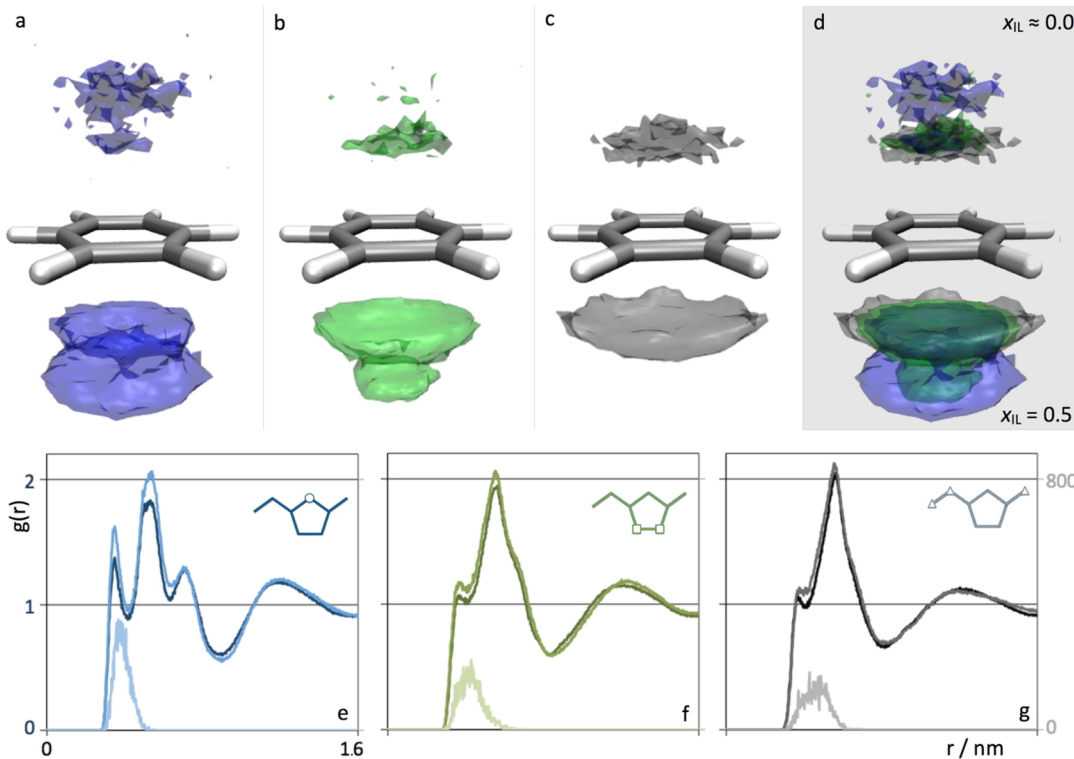


Figure 3. (a–d) Spatial distribution functions of C2 (a, blue), C5 (b, green), and C6 (c, gray) atoms of the cation around a central benzene molecule. The top iso-surfaces represent densities of those atoms 6 times greater than the corresponding average densities in mixtures with the IL at infinite dilution; the bottom iso-surfaces correspond to densities 2.2 above average in equimolar mixtures. (d) Superimposition of panels a–c. (e–g) Pair radial distribution functions, $g(r)$, between carbon atoms of the cation and the OBT atoms of the anion. The three shades of each color (C2: blue, C5: green, C7: gray) represent mixtures with $x_{IL} = 0.75$ (darker), $x_{IL} = 0.5$ (intermediate), and $x_{IL} \approx 0$ (lighter).

between 0.65 and ≈ 1.0 (shown in the graph) but unlike the case of Figure 2c, there is no inversion of the trend for the H2 proton shifts.

As mentioned before, the H2 is the most interactive center in the imidazolium cation. When the aromatic molecules start to be interspersed in the polar network of the ionic liquid, there will be a competition between the interactions with the oxygen atoms (OBT) of the $[\text{Ntf}_2]^-$ anion and the π electrons or fluorine atoms of the aromatic solute. This competition will differentiate the H2 from the H4 and H5 protons. Since the polar network is stronger at the H2–OBT contacts than at the H4/5–OBT contacts, the latter are the ones that will more likely break up when the aromatic molecules start to permeate (and partially disrupt) the IL polar network. This will lead to a higher proportion of H4 and H5 protons interacting with the solute molecules (relative to the H2 interactions) which can lead to the different shifts observed. In order to corroborate these assumptions, we have decided to extend our previous MD simulations whose structural analyses were based solely on the C2 atom of the imidazolium cation.

Figure 3 shows spatial distribution functions (SDFs) of C2, C5, and C6 atoms of the cation around a benzene molecule along with radial distribution functions (RDFs) of C2, C5, and C7 with the OBT atoms of the anion.

The figure shows that the distribution of the different carbon atoms around the aromatic plane of the benzene molecules is quite differentiated. The blue/green/gray isosurfaces represented below the aromatic rings in Figure 3a–c represent densities in equimolar (IL+benzene) mixtures larger than 2.2 times the average density of the C2, C5, and C7 atoms in the simulation box. One can see that the C2 atoms occupy

positions directly below (and also above since we are just looking at the bottom half of the symmetrical SDFs) the aromatic plane in a double-tier fashion that corresponds to the different orientations of the imidazolium ring relative to the aromatic ring. The C5 atom also occupies the same region in space, but the tier closer to the benzene molecule is larger than the one further away from it. Finally, the aliphatic C7 atoms occupy positions that are close to the aromatic plane but more off-center to the normal of it (C8 will occupy positions even more off-center). These distributions can be reconciled with the NMR signals if one recognizes that the largest shielding effects will be felt closer to the center of the normal to the aromatic ring: C2 shows the most centered distribution but part of the atoms are further away from the plane; C5 atoms are closer, but the closest tier also spreads further from the center; C7 (and other aliphatic atoms, namely C8) can lie quite close to the aromatic plane but occupy more peripheral positions. The balance between distance from the plane and location at a central position dictates the observed NMR shielding shifts ($\text{H2} \approx \text{H4/H5} > \text{H6/H7} > \text{H8}$, cf. Figure 2c) in the IL-rich phase of the (IL plus benzene) mixtures. Conversely, in benzene mixtures with $[\text{C}_2\text{C}_1\text{im}][\text{Ntf}_2]$ at almost infinite dilution (represented in Figure 3a–c by the isosurfaces depicted above the aromatic rings), one can see that in the case of the C2 atom, the tier closer to the ring almost vanishes, which is compatible with the trend inversion (large deshielding shift observed for the H2 atom in the $[\text{C}_2\text{C}_1\text{im}][\text{Ntf}_2]$ solutions at infinite dilution). The positioning of the C2 atoms further away from the center of the benzene aromatic plane can be rationalized if one takes into account the RDFs presented in Figure 3e–g. The correlation functions between the distance of

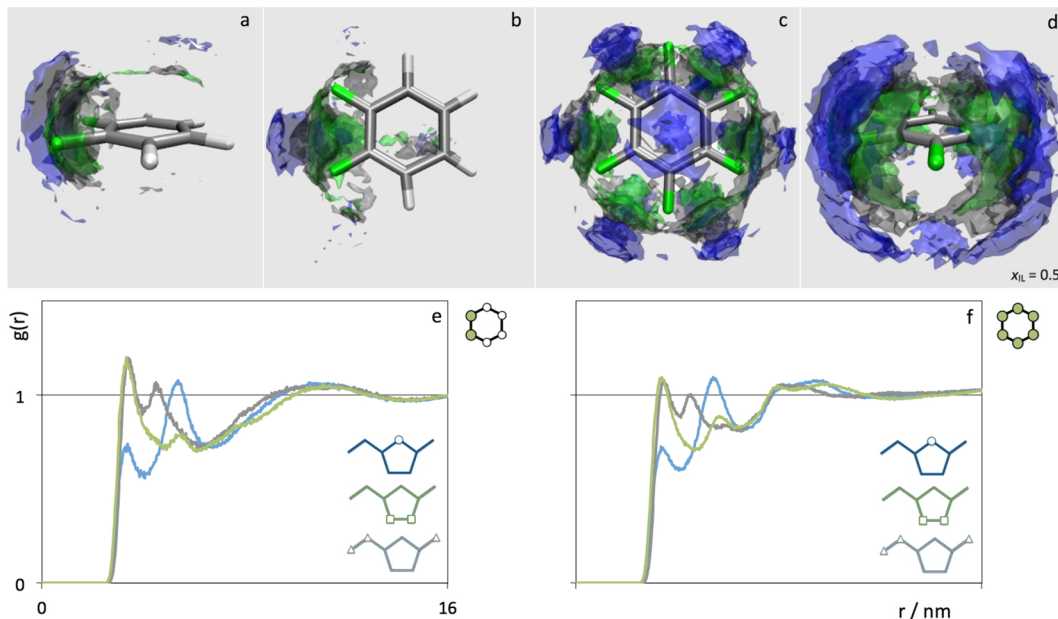


Figure 4. (a–d) Spatial distribution functions of C2 (blue), C5 (green), and C6 (gray) atoms around 1,2-difluorobenzene (a,b) or hexafluorobenzene (c,d) molecules in equimolar (IL+aromatic) mixtures. The iso-surfaces represent densities of 2.2 above average. (e–f) Pair radial distribution functions, $g(r)$, between carbon atoms of the cation (C2: blue, C5:green, C7: gray) and the fluorine atoms of the solute in equimolar mixtures of 1,2-difluorobenzene (e) and hexafluorobenzene (f).

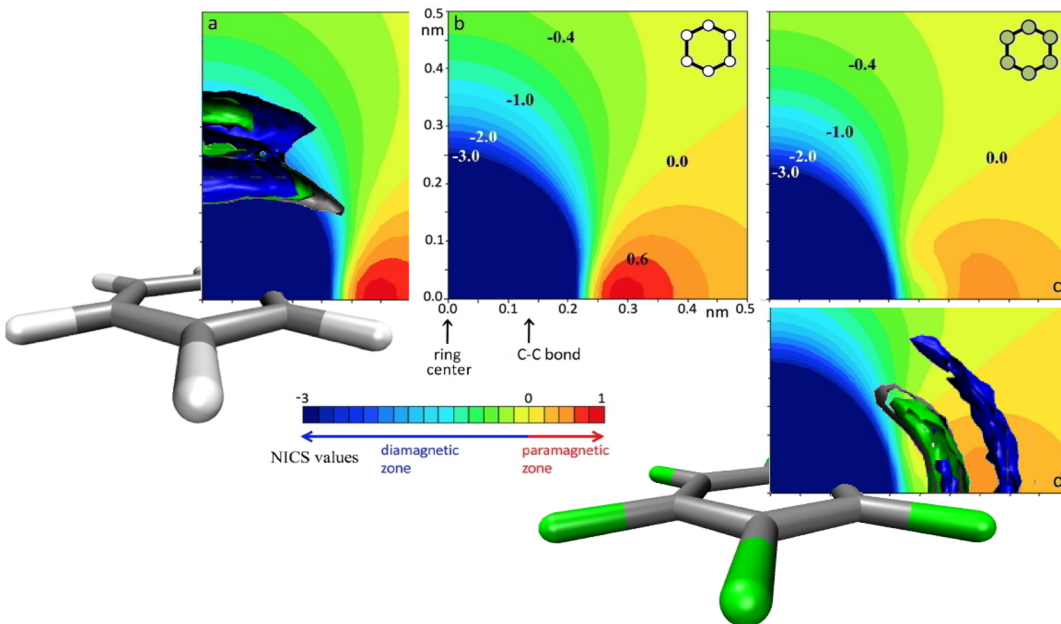


Figure 5. (a) Partial cross section of the SDFs of Figure 3d (bottom) superimposed on (b) NICS data¹⁴ for the paramagnetic and diamagnetic effects around a benzene molecule. (d) Partial cross section of the SDFs of Figure 4d superimposed on (c) NICS data¹⁴ for the paramagnetic and diamagnetic effects around a hexafluorobenzene molecule.

the different carbon atoms of the imidazolium ring and the nitrogen atom of the bistriflame anion show that the interactions between the two ions is more intense at the C2 position, especially at infinite dilution conditions: when an isolated ion pair is surrounded by benzene molecules, the anion and cation maintain a contact via the C2/H2 position of the latter. In those conditions, the H2 atom cannot lie close to the aromatic plane because it is interacting most of the time with the anion.

Figure 4 depicts the distribution of the different protons of the imidazolium cation around 1,2-difluorobenzene and hexafluorobenzene for equimolar mixtures. Figure 4a–d represents spatial distribution functions of selected imidazolium atoms around the fluorinated aromatic molecules and shows that the cations are predominantly positioned around the plane of the aromatic molecules (and not above and below it as in the case of the benzene mixtures). The figure also shows that the C4/5 atoms lie closer to the fluorine, followed by the aliphatic carbon atoms, and finally (further away from the ring) the C2

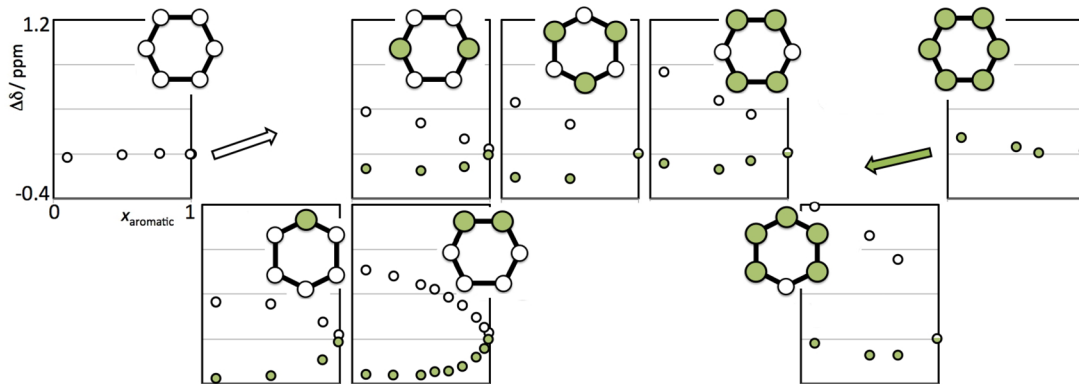


Figure 6. Deviations of the ^{13}C NMR shifts of different carbon atoms of the aromatic solutes, $\Delta\delta$, as a function of the concentration of eight (IL + aromatic) mixtures. The white circles denote hydrogenated carbon atoms; the green circles fluorinated ones. The grouping of the graphs in two tiers corresponds to symmetrical or asymmetrical solute molecules (those in the bottom tier can have nonequivalent fluorinated or hydrogenated carbon atoms). The white arrow represents the deshielding deviations felt by hydrogenated atoms as the solutes become more fluorinated; the green arrow indicates the shielding deviations experienced by the fluorinated carbon atoms as the solutes become less fluorinated (see text). Note that the NMR discussion based on the IL-components was based on ^1H shifts, while the corresponding discussion based on the aromatic components is based on ^{13}C shifts.

atoms. The RDFs depicted in Figure 4e,f corroborate such distribution: the correlations between the C4/C5 atoms and the fluorine atoms of the aromatic molecules are more intense and at closer distances than those corresponding to the aliphatic or the C2 carbon atoms. The privileged interactions between the fluorine atoms and the C4/C5 positions of the ring are again a consequence of the stronger interactions between the C2 position and the bis triflimate anions (the corresponding RDFs in IL plus fluorinated benzenes are similar to those already presented in Figure 3e–g).

At this point, there seems to be a contradiction between the NMR results and the MD data: For the very diluted IL mixtures in benzene, we have seen that the increasing order of shielding NMR shifts— $\text{H}_2 \approx \text{H}_8 < \text{H}_6/\text{H}_7 < \text{H}_4/\text{H}_5$ —could be justified by the corresponding distances to the center of the benzene ring along the direction perpendicular to the aromatic plane. In other words, the H4/H5 atoms occupied positions closer to the ring at its polar and diamagnetic positions and therefore exhibited larger shielding shifts. In the case of the fluorinated benzene mixtures, the H4/H5 atoms still occupy positions closer to the ring but now in a direction parallel to the aromatic plane (equatorial, paramagnetic positions). Thus, they should exhibit the largest deshielding shifts, in conflict with the experimental NMR results, which still show the largest shielding effects.

Fortunately, such inconsistency is just a consequence of a superficial analysis that simply associates diamagnetic aromatic behavior with positions normal to the aromatic plane and paramagnetic behavior with positions within that plane. Recently, Korenaga et al.¹⁴ estimated the NMR shielding effects around benzene and fluorinated benzene molecules using nucleus-independent chemical shift (NICS) calculations at the GIAO/B3LYP/6-311++G(2d,p) level. Figure 5 was built by superimposing our own SDF results for the $[\text{C}_2\text{C}_1\text{im}][\text{Ntf}_2]$ plus benzene and $[\text{C}_2\text{C}_1\text{im}][\text{Ntf}_2]$ plus hexafluorobenzene equimolar mixtures with the above-mentioned NICS data (as depicted in Figure 2 of ref 14).

Figure 5a confirms that for equimolar (IL plus benzene) mixtures, the cations are positioned along the normal of the aromatic plane. The C4/C5 and also the C2 atoms in the tier closer to the ring lie deep inside the diamagnetic zone of the

benzene molecule (the situation is drastically modified for C2 at infinite dilution in benzene due to the depletion of the closest tier), whereas the aliphatic carbons lie in the more peripheral and less diamagnetic zones around the normal of the plane.

Conversely, Figure 5d depicts the behavior for equimolar (IL plus hexafluorobenzene) mixtures where the cations are now positioned around the aromatic plane. Such regions are characterized by a nonmonotonous behavior of the magnetic shielding effects, with the intensity and position of the most paramagnetic zones differing for benzene and hexafluorobenzene (cf. Figure 5b,c): Figure 5c shows that the regions closer to the aromatic ring within the aromatic plane are not necessarily the most paramagnetic. In fact, Figure 5d shows that the C2 atoms of the cation that occupy positions further away from the ring experience a more paramagnetic influence than their C4/C5 counterparts. This is consistent with the NMR results.

The shielding/deshielding effects within the mixtures can also be probed in the aromatic molecules using ^{13}C NMR data on the carbon atoms of the aromatic rings (^1H or ^{19}F NMR would also be a possibility but it would not encompass all studied aromatic compounds (there are no fluorine atoms in benzene or hydrogen atoms in hexafluorobenzene)). Figure 6 shows the ^{13}C NMR chemical shift differences between the mixtures and the corresponding pure aromatic compounds. Again a positive shift means that the carbon atoms in the mixtures are experiencing a more deshielded (downfield) environment, whereas the opposite (upfield, shielding shifts in the mixtures) is true for the negative values.

The overall trends are clear: the carbon atoms attached to hydrogen atoms (white circles) experience small shielding shifts in the benzene mixtures that change to progressively larger deshielding shifts in mixtures with more fluorinated aromatic molecules; the carbon atoms connected to fluorine atoms (green circles) experience deshielding shifts in the hexafluorobenzene mixtures that become progressively large shielding shifts in mixtures with less fluorinated aromatic molecules. The trends are easily explained if one considers that, as the aromatic mixtures become more diluted, the environment of a given aromatic molecule starts to be depleted in other aromatic

molecules and enriched in the ions of the IL. As we have seen before, the positions in front of the aromatic hydrogen atoms will be occupied by the most electronegative atoms of the anions (leading to deshielding effects and downfield shifts), whereas those in the vicinity of the aromatic fluorine atoms will be occupied by the most electropositive atoms of the cations (leading to shielding effects and upfield shifts). Those shifts will be more intense (hence the trends along the aromatic series) if the molecule has fewer of a given type of site (fluorinated or hydrogenated) since the relative concentration of IL ions around that position will be larger. Regarding each individual system, the larger variations in chemical shift observed in the carbons bonded to hydrogen atoms (in all cases except fluorobenzene), are also consistent with the more localized character of the anion-hydrogen interaction, in comparison with the cation-fluorine one, already suggested in the previous work.¹ Finally, the only thing that needs to be explained are the small shielding shifts in benzene and the small deshielding shifts in hexafluorobenzene. In both cases, the shifts were expected to be small (the cations or anions will be less concentrated among the all-hydrogenated or all-fluorinated sites) but with the opposite sign: in benzene there will be anions around the aromatic plane causing small deshielding shifts; in hexafluorobenzene there will be cations causing shielding shifts. The apparent contradiction can be resolved by taking into account the fact that in the case of benzene there will be a large concentration of (aromatic) cations above and below the aromatic plane of benzene. Figure 7 shows a molecular representation of the two closest cations to an aromatic ring in a equimolar inclusion crystal of $[C_2C_1im][Ntf_2] \cdot C_6H_6$.¹⁵

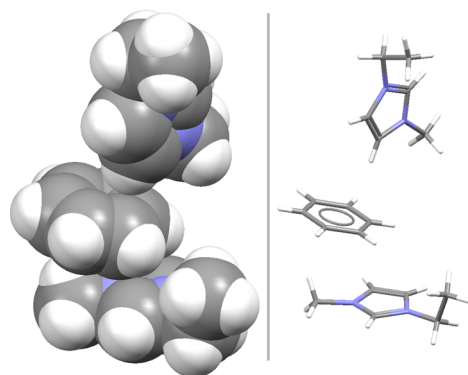


Figure 7. Orientation of the imidazolium cations in the first coordination shell of a benzene molecule in a equimolar $[C_2C_1im][Ntf_2] \cdot C_6H_6$ inclusion crystal (built from the CIF file deposited at the CCDC database).¹⁵

As expected, the imidazolium cations occupy positions above and below the plane. One of them has its aromatic plane perpendicular to the benzene plane (and its C4/C5 atoms closer to benzene), whereas the other is oriented parallel to the benzene plane. This last ion will be able to cause a large shielding shift in the carbon atoms of the benzene molecule due to the diamagnetic influence of its delocalized aromatic electron cloud.

Additional experimental information about the liquid structure in the studied systems was also obtained by the 2D $^1H-^1H$ NOESY method. Recently, Gabl et al. proposed a new model theory to interpret the results from intermolecular NOEs in solutions.¹⁶ They addressed, as proposed earlier by

Frezzato et al.,¹⁷ that the intermolecular NOE should be dominated by long-range dipolar couplings instead of the previously accepted interpretation that it correlates signals mainly arising from protons that are close in space (within 0.5 nm) for a significant amount of time. This finding resembles the theory presented by Halle, which predicts that the intermolecular NOE in protein–water solutions is dominated by long-range couplings to bulk water rather than those to hydration water.¹⁸ As a consequence of this new theory, the information provided by site-specific NOE in solution, and also in ILs, can not be interpreted solely in terms of local structure: instead, it provides information about the mean molecular orientation over long distances.

Here, the 2D NOESY spectra provide information about the dominant molecular orientations organization in the binary mixtures and the way it is affected by the nature of the aromatic compounds. In Figure 8, 2D NOESY spectra of the equimolar mixtures of $[C_2C_1im][Ntf_2]$ with benzene, 1,4-difluorobenzene and pentafluorobenzene are shown; for simplicity, only the region of the intermolecular cross-peaks, between the aliphatic protons of the cation (vertical axis) and the protons of the aromatic molecules (horizontal axis), is displayed.

It is interesting to note the existence in all mixtures of a cross peak between the H8 protons of the IL and the protons of the aromatic molecule. The mixture with benzene, in particular, shows only this cross peak, in agreement with Figure 3 where the aliphatic protons of the cation (and H8 in particular) occupy preferably positions which are more off-center to the normal of the aromatic planes. In the other mixtures, the results also show a correlation between the mean relative orientations between the aromatic protons of the IL and those of the aromatic molecules—a consequence of the shift in the positioning of the cations, from completely axial to equatorial positions.

CONCLUSION

It was shown previously¹ that the mutual solubilities of $[C_2C_1im][Ntf_2]$ and aromatic molecules (benzene and its fluorinated derivatives) could be correlated to the dipolar and quadrupolar moments of the latter and that this reflected the charge-induced structuration of the IL ions around the aromatic molecules. Ab initio calculations¹ also established that the aromatic quadrupole moment, Q_{zz} , of those aromatic molecules is an almost linear function of the number of fluorine substitutions.

In this paper we were able to demonstrate that we can follow the above-mentioned structural changes using different NMR-based techniques. As a coda, one can show that the chemical shift variation of the protons of the imidazolium ring varies with the aromatic quadrupole moment. Such relations between $\Delta\delta(H2)$ and Q_{zz} (or the number of fluorine atoms substituted in the aromatic molecules) are shown in Figure 9.

Negative $\Delta\delta(H2)$ values correspond to mixtures containing hydrogenated aromatics with low (negative) Q_{zz} values. With the progressive fluorination of the aromatic molecules and concomitant increase of their aromatic quadrupole moments, the $\Delta\delta(H2)$ values start to increase and reach an almost constant value for mixtures containing benzene molecules substituted with three or more fluorine atoms. This effect is fully in agreement with the discussion regarding the spatial arrangements in these mixtures: in benzene the cations are mainly located above and below the aromatic plane, experiencing the diamagnetic influence of the aromatic

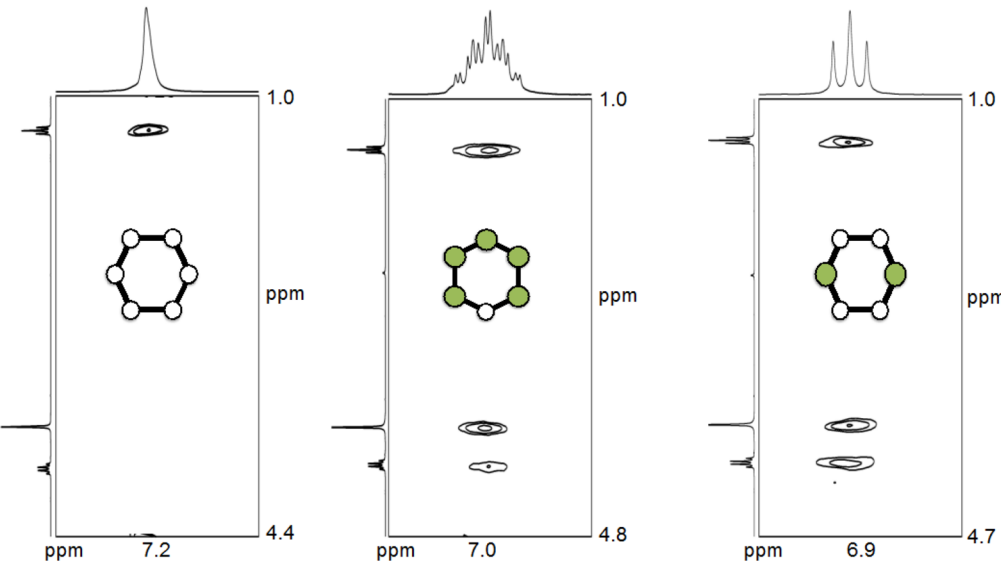


Figure 8. Partial 2D ^1H - ^1H NOESY spectra of the equimolar mixtures of IL with benzene (left), pentafluorobenzene (middle) and 1,4-difluorobenzene (right). Mixing times of 600 ms. The peaks in the vertical axes correspond (from top to bottom) to the H8, H6 and H7 aliphatic hydrogen atoms of $[\text{C}_2\text{C}_1\text{im}]^+$; those in the horizontal axes refer to the aromatic protons of the aromatic solutes (all hydrogen atoms are equivalent in each aromatic compound).

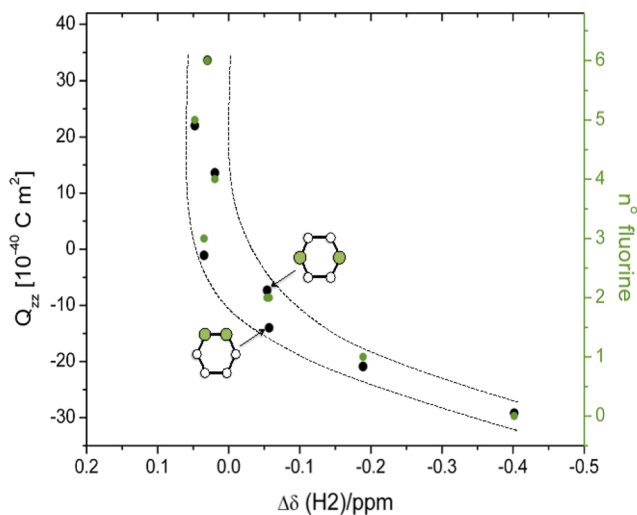


Figure 9. Relations between the chemical shift variation of H2, $\Delta\delta(\text{H}2)$, the number of fluorine atoms in the aromatic solutes, and the value of the corresponding aromatic quadrupole moments, Q_{zz} . The $\Delta\delta(\text{H}2)$ data correspond to (IL+aromatic solute) equimolar mixtures.

electrons; as the aromatic ring progressively becomes more fluorinated, the cations migrate to the equatorial plane of the aromatic molecule, to a region of milder paramagnetic effect.

Subtler effects can also be seen in Figure 9, such as on the behavior of the mixtures containing the two (1,2- and 1,4-) difluorobenzene isomers. Although their $\Delta\delta(\text{H}2)$ values are almost identical, their Q_{zz} values are quite distinct: $Q_{zz}(1,4-) = -7.3 \times 10^{-40} \text{ C m}^2$ and $Q_{zz}(1,2-) = -14 \times 10^{-40} \text{ C m}^2$. The lower aromatic quadrupole moment of 1,2-difluorobenzene is related to the existence of a strong dipole moment in the molecule that, in turn, is a consequence of the overall (asymmetrical) distribution of its fluorine atoms. This causes a different distribution of the IL ions around each isomer (as seen in Figures 3 and 8 of ref 1) but will have little impact on the specific local interactions between the two fluorine atoms of

the aromatic solute and the aromatic hydrogen atoms of the IL cation.

AUTHOR INFORMATION

Notes

The authors declare no competing financial interest.

ACKNOWLEDGMENTS

Financial support provided by Fundação para a Ciência e Tecnologia (FCT) through projects FCT-ANR/CTM-NAN/0135/2012 (including the postdoctoral grant of K.S.), PTDC/CTM-NAN/121274/2010, and PEst-OE/QUI/UI0100/2013. P.M. acknowledges postdoctoral grant SFRH/BPD/81748/2011. F.V.C. thanks FCT for financial support through the project PEst-OE/FIS/UI0261/2011-2013.

REFERENCES

- (1) Shimizu, K.; Costa Gomes, M. F.; Pádua, A. A. H.; Rebelo, L. P. N.; Canongia Lopes, J. N. On the Role of the Dipole and Quadrupole Moments of Aromatic Compounds in the Solvation by Ionic Liquids. *J. Phys. Chem. B* **2009**, *113*, 9894–9900.
- (2) Shimizu, K.; Bernardes, C. E. S.; Canongia Lopes, J. N. The complex structure of ionic liquids at an atomistic level: From “red-and-greens” to charge templates. *Pure Appl. Chem.* **2014**, *86*, 119–133.
- (3) Zheng, Y.-Z.; Wang, N.-N.; Luo, J.-J.; Zhou, Y.; Yu, Z.-W. Hydrogen-bonding interactions between $[\text{BMIM}]^+[\text{BF}_4]^-$ and acetonitrile. *Phys. Chem. Chem. Phys.* **2013**, *15*, 18055–18064.
- (4) Avent, A. G.; Chaloner, P. A.; Day, M. P.; Seddon, K. R.; Welton, T. Evidence for hydrogen bonding in solutions of 1-ethyl-3-methylimidazolium halides, and its implications for room-temperature halogenoaluminate(III) ionic liquids. *J. Chem. Soc., Dalton Trans.* **1994**, 3405–3413.
- (5) Bonhôte, P.; Dias, A. P.; Papageorgiou, N.; Kalyanasundaram, K.; Grätzel, M. Hydrophobic, Highly Conductive Ambient-Temperature Molten Salts. *Inorg. Chem.* **1996**, *35*, 1168–1178.
- (6) Mele, A.; Romano, G.; Giannone, M.; Ragg, E.; Fronza, G.; Raos, G.; Marcon, V. The Local Structure of Ionic Liquids: Cation–Cation NOE Interactions and Internuclear Distances in Neat $[\text{BMIM}]^+[\text{BF}_4]^-$ and $[\text{BDMIM}]^+[\text{BF}_4]^-$. *Angew. Chem., Int. Ed.* **2006**, *45*, 1123–1126.

- (7) Marincola, F. C.; Piras, C.; Russina, O.; Gontrani, L.; Saba, G.; Lai, A. NMR Investigation of Imidazolium-Based Ionic Liquids and Their Aqueous Mixtures. *ChemPhysChem* **2012**, *13*, 1339–1346.
- (8) Headley, A. D.; Jackson, N. M. The effect of the anion on the chemical shifts of the aromatic hydrogen atoms of liquid 1-butyl-3-methylimidazolium salts. *J. Phys. Org. Chem.* **2002**, *15*, 52–55.
- (9) Shiflett, M. B.; Yokozeki, A. Liquid–Liquid Equilibria in Binary Mixtures Containing Fluorinated Benzenes and Ionic Liquid 1-Ethyl-3-methylimidazolium Bis(trifluoromethylsulfonyl)imide. *J. Chem. Eng. Data* **2008**, *53*, 2683–2691.
- (10) Canongia Lopes, J. N.; Deschamps, J.; Pádua, A. A. H. Modeling ionic liquids using a systematic all-atom force field. *J. Phys. Chem. B* **2004**, *108*, 2038–2047.
- (11) Canongia Lopes, J. N.; Pádua, A. A. H. Molecular Force Field for Ionic Liquids Composed of Triflate or Bistriflylimide Anions. *J. Phys. Chem. B* **2004**, *108*, 16893–16898.
- (12) Jorgensen, W. L.; Maxwell, D. S.; Tirado-Rives, J. Development and Testing of the OPLS All-Atom Force Field on Conformational Energetics and Properties of Organic Liquids. *J. Am. Chem. Soc.* **1996**, *118*, 11225–11236.
- (13) Smith, W.; Forester, T. R. *The DL_POLY Package of Molecular Simulation Routines (v.2.2)*; The Council for The Central Laboratory of Research Councils, Daresbury Laboratory: Warrington, U.K., 2006.
- (14) Korenaga, T.; Kobayashi, F.; Nomura, K.; Sakai, T.; Shimada, K. The shielding effect of fluoroaromatic rings in NMR. *J. Fluorine Chem.* **2013**, *156*, 1–4.
- (15) Łachwa, J.; Bento, I.; Duarte, M. T.; Canongia Lopes, J. N.; Rebelo, L. P. N. Condensed phase behaviour of ionic liquid–benzene mixtures: Congruent melting of a [emim][NTf₂]·C₆H₆ inclusion crystal. *Chem. Commun.* **2006**, 2445–2447.
- (16) Gabl, S.; Steinhauser, O.; Weingärtner, H. From Short-Range to Long-Range Intermolecular NOEs in Ionic Liquids: Frequency Does Matter. *Angew. Chem., Int. Ed.* **2013**, *52*, 9242–9246.
- (17) Frezzato, D.; Rastrelli, F.; Bagno, A. Nuclear Spin Relaxation Driven by Intermolecular Dipolar Interactions: The Role of Solute–Solvent Pair Correlations in the Modeling of Spectral Density Functions. *J. Phys. Chem. B* **2006**, *110*, 5676–5689.
- (18) Halle, B. Cross-relaxation between macromolecular and solvent spins: The role of long-range dipole couplings. *J. Chem. . Phys.* **2003**, *119*, 12372–12385.